Supporting Information

Introducing visible-light sensitivity into photocatalytic CeO_2 nanoparticles by hybrid particle preparation exploiting plasmonic properties of gold: Enhanced photoelectrocatalysis exemplified for hydrogen peroxide sensing

Shuang Zhao[1], Marc Riedel[2], Javier Patarroyo[3], Neus Bastus[3], Victor Puntes[3,4,5], Zhao Yue[6*], Fred Lisdat[2*], Wolfgang J. Parak[1,7*]

[1]Fachbereich Physik, CHyN, Universität Hamburg, 22761, Hamburg, Germany
[2]Biosystems Technology, Institute of Life Sciences and Biomedical Technologies, Technical University of Applied Sciences Wildau, 15745, Wildau, Germany
[3]Institut Català de Nanociència i Nanotecnologia (ICN2), CSIC and BIST, Campus UAB, Bellaterra, 08193, Barcelona, Catalonia, Spain
[4]Vall d'Hebron Institut de Recerca (VHIR), 08035, Barcelona, Catalonia, Spain
[5]ICREA, Pg. Lluís Companys 23, 08010, Barcelona, Catalonia, Spain
[6]Department of Microelectronics, Nankai University, 30071, Tianjin, China
[7]CIC Biomagune, 20014, San Sebastian, Spain
[*]corresponding authors: yuezhao@nankai.edu.cn, flisdat@th-wildau.de, wolfgang.parak@uni-hamburg.de

I) Synthesis and characterization of nanoparticles

Materials for nanoparticle (NP) synthesis: Cerium(III) nitrate hexahydrate (99% trace metals basis), gold(III) chloride trihydrate (99% trace metals basis), silver nitrate (ACS reagent, >99.8%), potassium carbonate (ACS reagent, >99.0%), sodium citrate tribasic dihydrate (ACS reagent, >99.0%), tannic acid (ACS reagent), hydrogen peroxide (H_2O_2), cysteamine, poly(diallyldimethylammonium chloride) solution (PDDA), ascorbic acid, uric acid, dopamine, glucose, NaCl, KCl, and phosphate buffered saline tablets (PBS, pH 7.4 at 25℃) were purchased from Sigma-Aldrich (Steinheim, Germany). HCl and NaOH were obtained from ROTH (Karl Roth, Germany). There was not further purification of the reagents after receiving. Milli-Q water was used for all the aqueous solutions in this work.

Structural characterization: Transmission electron microscopy (TEM) images are shown in Figure SI-1 and Figure SI-2. X-ray diffraction (XRD) characterization is presented in Figure SI-4. Further characterization is available in a previous report [1].

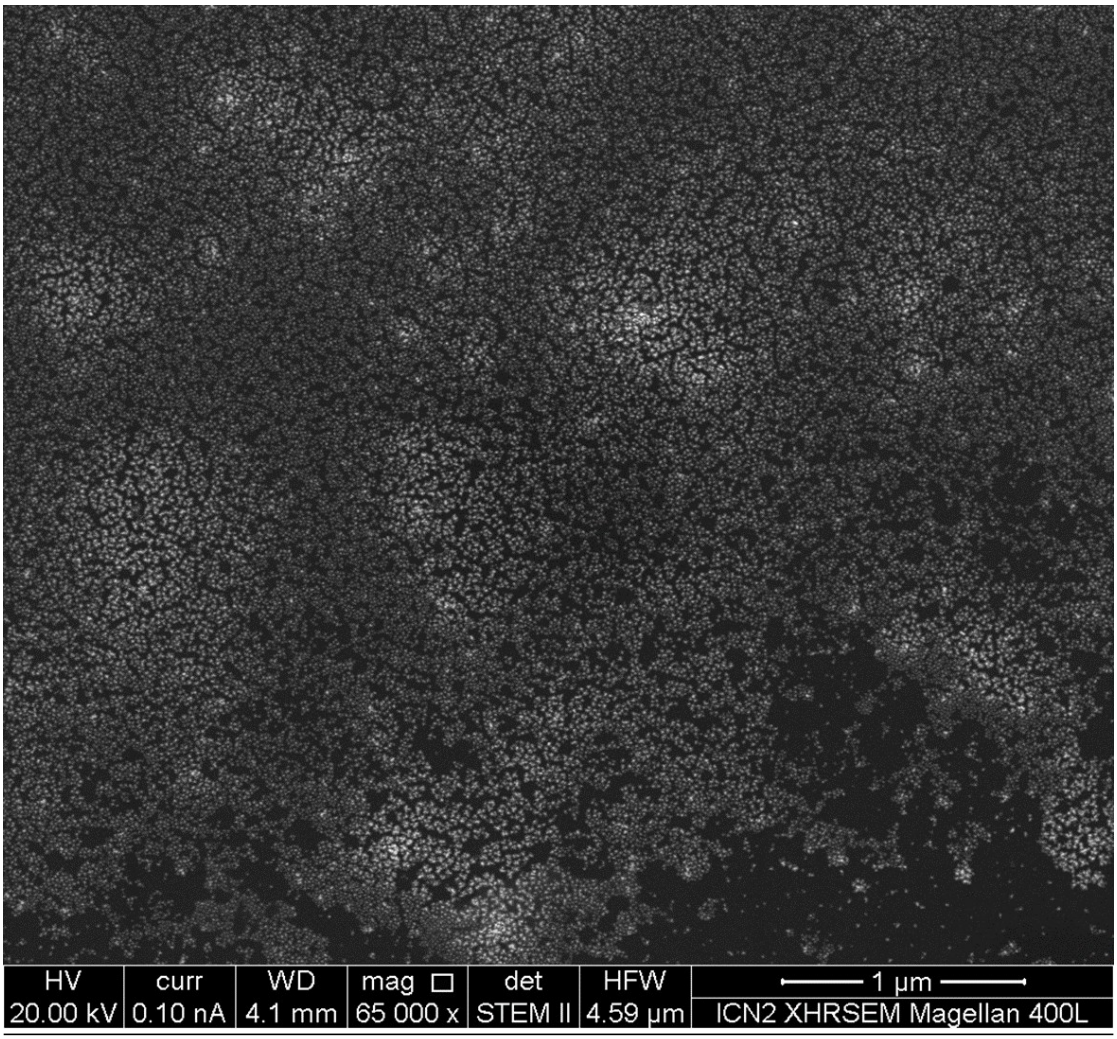

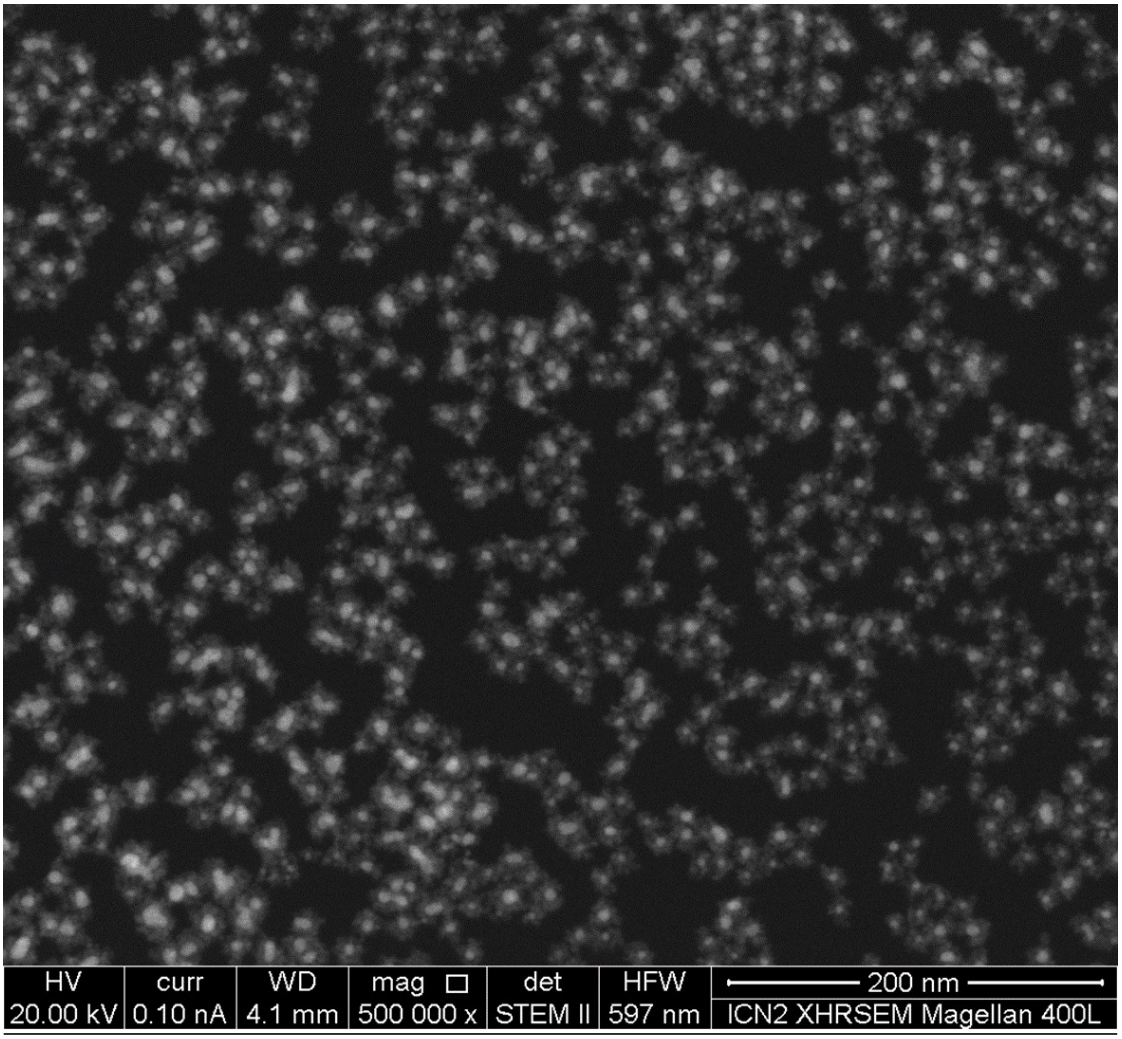

Figure SI-1: *Representative high-angle annular dark field scanning TEM (HAADF-STEM) images of as-obtained colloidal Au@CeO_2 hybrid NPs, revealing the formation of a core of Au (~5 nm) surrounded by a relatively uniform CeO_2 shell.*

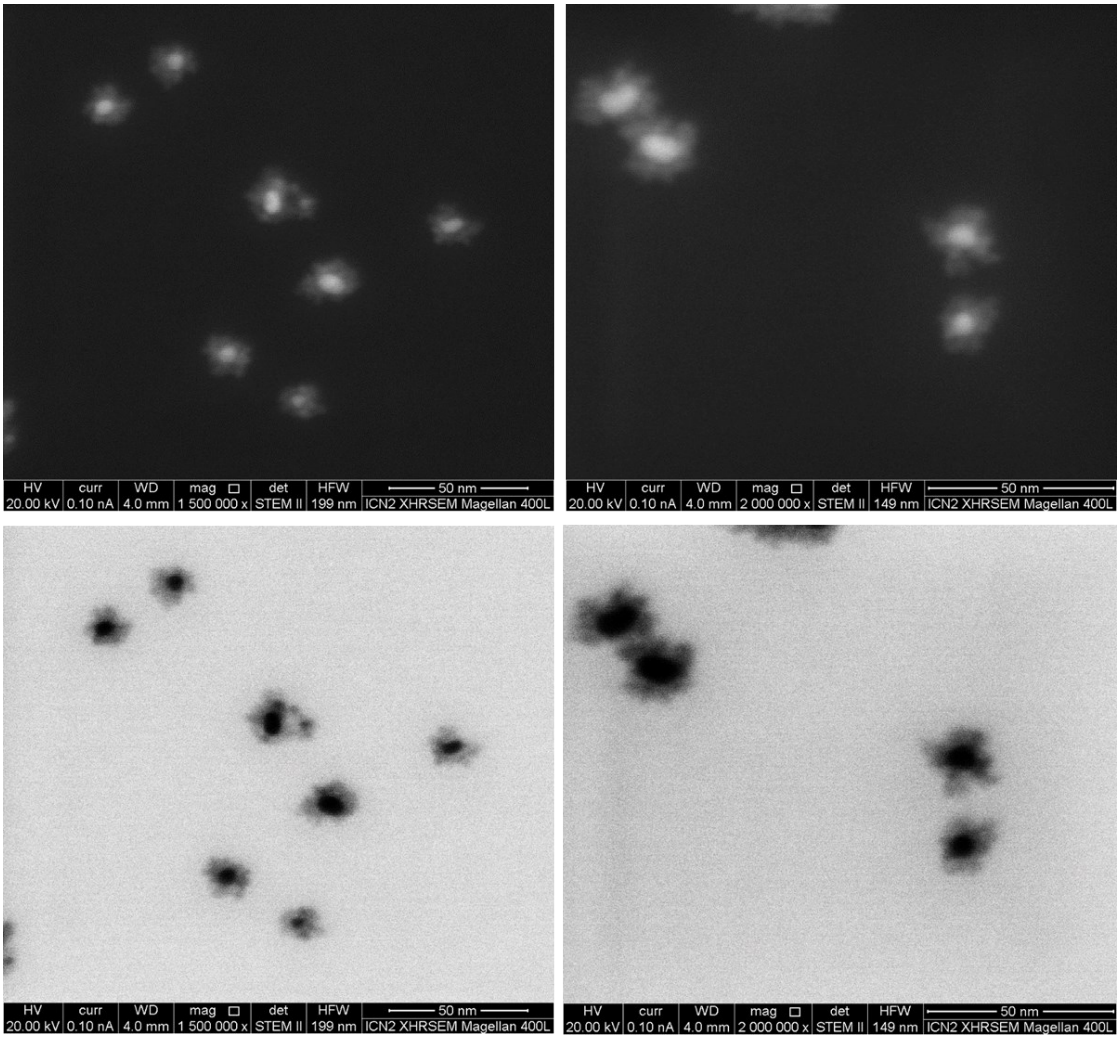
HV curr WD mag □ det HFW 50 nm
20.00 kV 0.10 nA 4.0 mm 1 500 000 x STEM II 199 nm ICN2 XHRSEM Magellan 400L
HV curr WD mag □ det HFW 50 nm
20.00 kV 0.10 nA 4.0 mm 2 000 000 x STEM II 149 nm ICN2 XHRSEM Magellan 400L
HV curr WD mag □ det HFW 50 nm
20.00 kV 0.10 nA 4.0 mm 1 500 000 x STEM II 199 nm ICN2 XHRSEM Magellan 400L
HV curr WD mag □ det HFW 50 nm
20.00 kV 0.10 nA 4.0 mm 2 000 000 x STEM II 149 nm ICN2 XHRSEM Magellan 400L

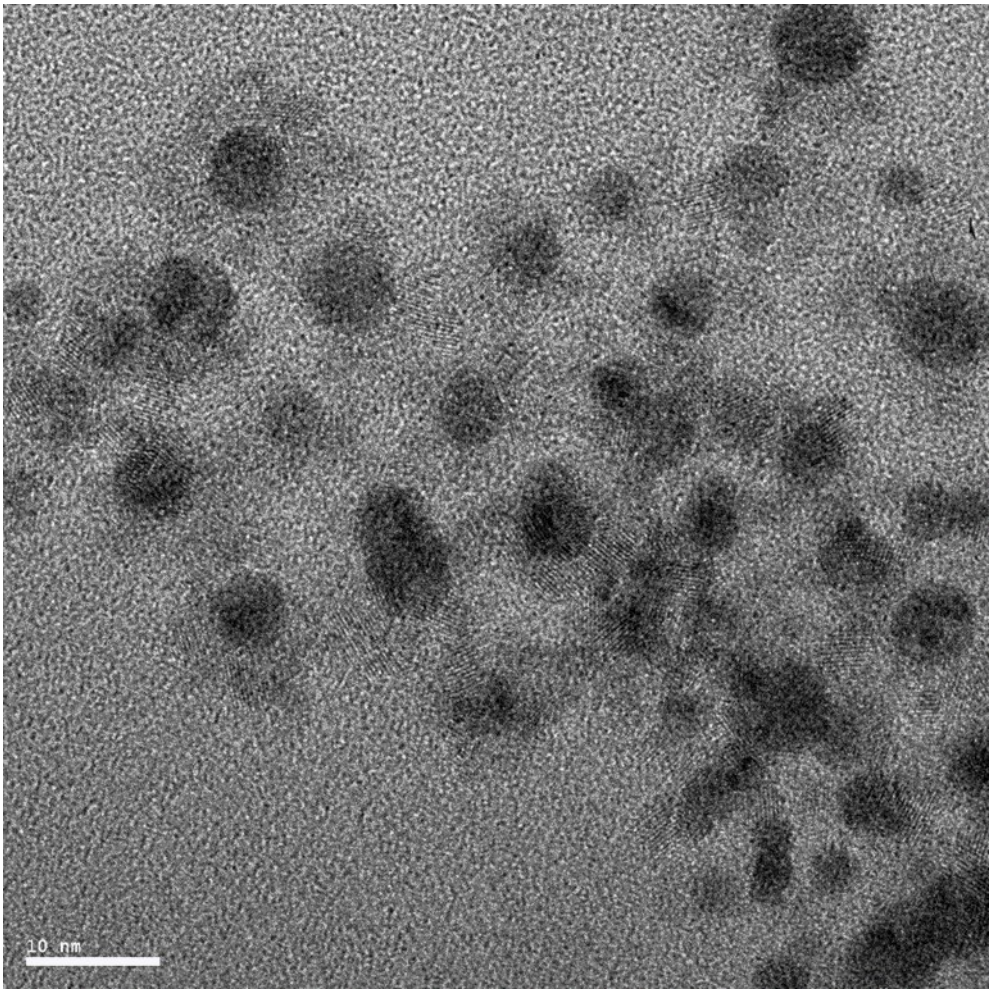

Figure SI-2: *High-resolution TEM (HRTEM) images revealing the details of the CeO_2 shell, which is composed of small NPs with sizes around 3-4 nm closely bound to the Au core.*

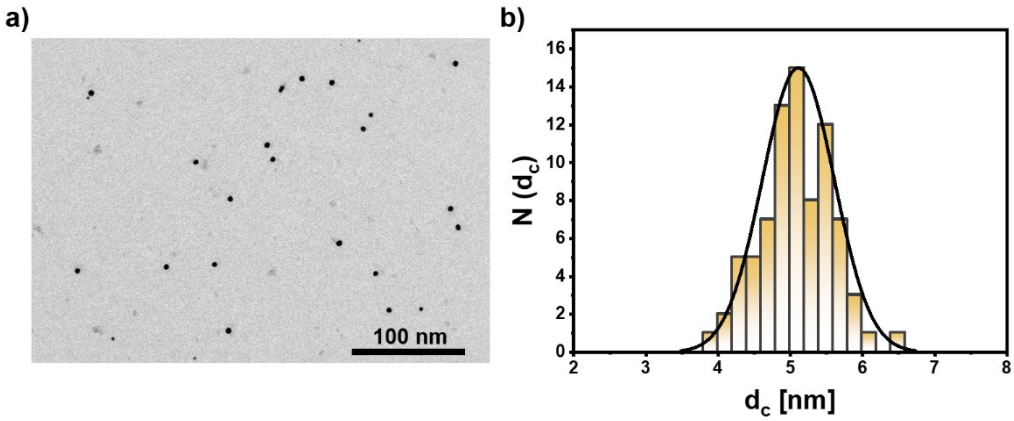

Figure SI-3: *TEM image of pure Au NPs and (b) the related size distribution $N(d_c)$ histograms from the core diameter (d_c) of the NPs. The mean diameter of the pure Au NPs is d_c = 5.1 ± 0.5 nm. This corresponds well to the size of the Au part of the Au@CeO_2 hybrid NPs.*

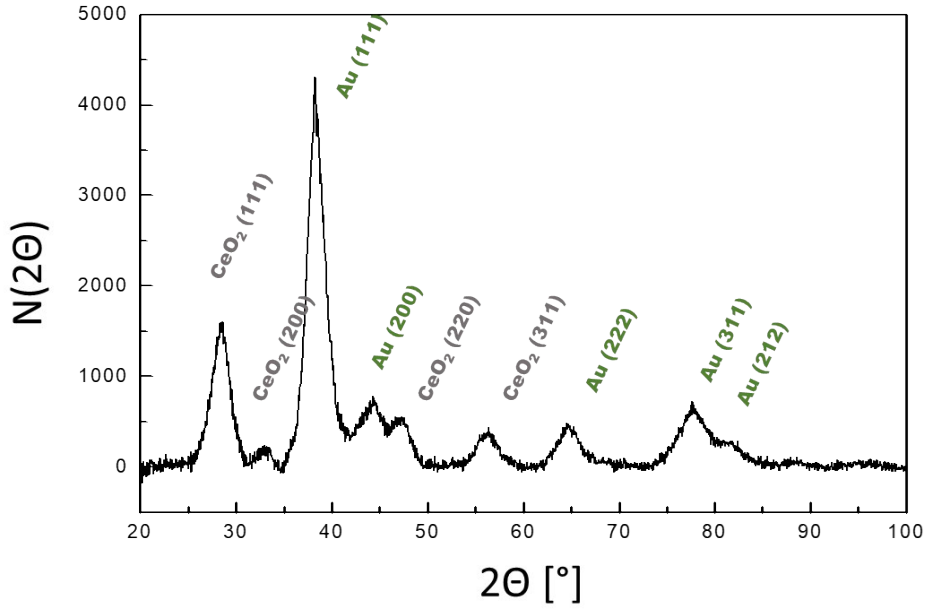

Figure SI-4: *Number of counts N of the X-ray diffraction (XRD) in dependence of the angle Θ of hybrid Au@CeO_2 NPs. Two series of sets of diffraction peaks are present, which are assigned to the fluorite (cubic) CeO2 phase (JCPDS No 34-0394) and to the cubic Au phase (JCPDS No 04-0784). The diffraction peaks of the Au core are sharp and intense, while those of CeO_2 are broad and weak, accordingly with the small crystalline size of the CeO_2 nanoparticles composing the shell.*

Optical NP characterization in water: The NPs were characterized in water by UV/VIS-absorption spectra and fluorescence spectroscopy. Absorption spectra showed a plasmon peak around 540 nm in the hybrid Au/CeO_2 core/shell NPs, in addition to the absorption of the CeO_2 NPs, which originates from the Au cores (Figure SI-5a). The fluorescence of Au/CeO_2 core/shell NPs showed the same peak as the pure CeO_2 NPs, and thus originates from the CeO_2 shell (Figure SI-5b). As control, Au NPs with similar size as the Au cores in the hybrid Au/CeO_2 core/shell NPs were prepared. The Au NPs had an absorption peak similar to the Au cores of the Au/CeO_2 hybrid NPs (Figure SI-5c).

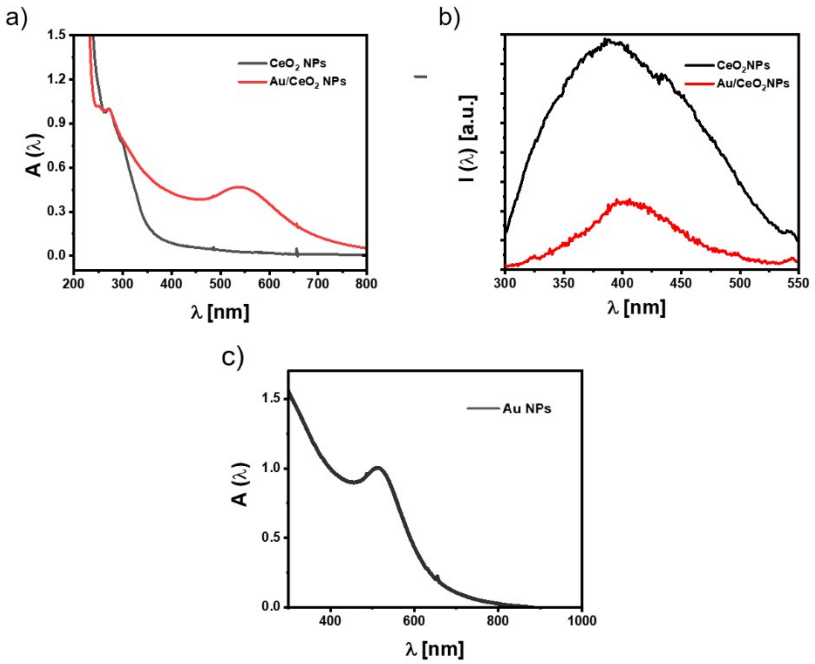

Figure SI-5: *a) Absorption and b) fluorescence spectra (with excitation at 290 nm) of pure CeO_2 and hybrid Au/CeO_2 NPs in water. Spectra were recorded in quartz cuvettes. c) Absorption spectrum of Au NPs in water.*

Colloidal NP characterization in water: The NPs were characterized in water by a Malvern Zetasizer combining dynamic light scattering (DLS) and Laser Doppler Anemometry (LDA). The hydrodynamic diameters d_h of the three types of NPs were determined by DLS as 20 nm for the pure CeO_2 NPs, 15 nm for the Au/CeO_2 NPs, and 6 nm for the Au NPs. The DLS data are shown in Figure SI-6. The zeta-potentials ζ as determined with LDA are shown in Table SI-1.

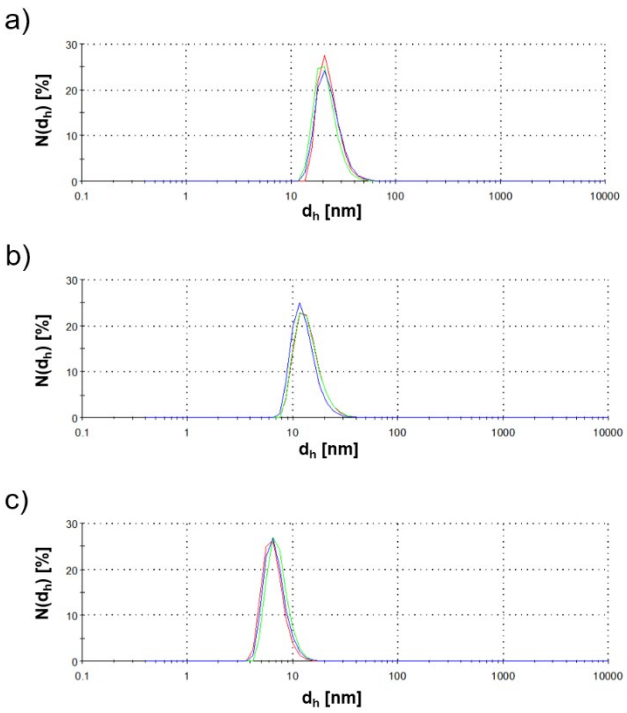

Figure SI-6: DLS number distribution $N(d_h)$ of the hydrodynamic diameters d_h of a) pure CeO_2 NPs, b) hybrid Au/CeO_2 NPs, and c) Au NPs.

NP type	ζ [mV]
CeO_2	-39.7 ± 1.67
Au/CeO_2	-42.9 ± 0.1

Table SI-1: Zeta potential ζ of pure CeO_2, and hybrid Au/CeO_2 NPs, as recorded in water with LDA.

Working electrodes: The working electrodes used in this work were 1 cm × 1 cm gold chips. The structure layout was 500 µm glass/20 nm Ti/200 nm Au (Suzhou Research Materials Microtech Co. Ltd, China). In the measurements, the Au area exposed to the solution is $A_{chip} \approx 0.28$ cm^2 based on a circular electrochemical cell with 0.6 cm diameter.

II) Characterization of nanoparticle deposition in a flow system with quartz crystal microbalance measurements

Firstly, the mass of per NP was calculated by using the bulk densities ρ_{Au} =19.32 g/cm³ and ρ_{CeO2} =7.22 g/cm³, and the core diameter d_c (*i.e.* the inorganic NP part without the organic surface coating) as determined by transmission electron microscopy (TEM, cf. Figure 1 in the main article. For Au/CeO_2 NPs, when the NPs are assumed as a perfect sphere (cf. Figure SI-7), the volume of one Au core can be calculated as V_{Au} = $4/3\times\pi\times(d_c(Au)/2)^3$ = 96.9 nm³. Based on this, the volume of the CeO_2 shell can be calculated as V_{CeO2} = $4/3\times\pi\times((d_c(Au/CeO_2)/2)^3-(d_c(Au)/2)^3)$ = 853.4 nm³.[2] Thus, the mass of one Au/CeO_2 NP (excluding the organic surface coating) is estimated to $m_{Au/CeO2}=\rho_{Au}\times V_{Au}+\rho_{CeO2}\times V_{CeO2}$ = 8.034×10^{-18} g. For the CeO_2 NPs, the volume of one CeO_2 core is V_{CeO2} = $4/3\times\pi\times(d_c(CeO_2)/2)^3$ = 1595.4 nm³. Thus, the mass of one CeO_2 NP is $m_{CeO2}=\rho_{CeO2}\times V_{CeO2}$ = 11.5×10^{-18} g.

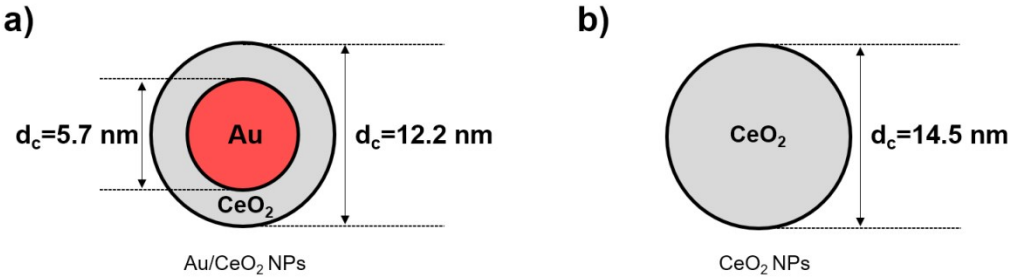

Figure SI-7: Sketch, showing the dimensions of the Au/CeO_2 NPs and CeO_2 NPs, as derived with TEM.

The amount of NPs adsorbed to the surfaces (such as the Au electrodes) was determined by quartz crystal microbalance (QCM) measurements. In the case the energy dissipation parameters change (ΔD) is less than 10^{-6} per 5 Hz of frequency change (Δf), the mass loaded is proportional to the frequency change according to the Sauerbrey relation: $\Delta m' = -C\cdot\Delta f/n$, where $\Delta m'$ is the mass change normalized to the surface area, C = 17.7 ng·$Hz^{-1}cm^{-2}$, and n is the overtone number.[3] The Sauerbrey relation was used in this way for the calculation of the mass change $\Delta m'$ on a gold surface due to the adsorption of NPs. The experimentally determined frequency changes as shown in Figure SI-8 are Δf_{CeO2} = -(14.343 ± 0.096) Hz ($\Delta D = 0.9\times10^{-6}$, $\Delta D/\Delta f < 0.5\times10^{-6}$ Hz), and $\Delta f_{Au/CeO2}$ = -(7.96 ± 0.18) Hz ($\Delta D = 0.92\times10^{-6}$, $\Delta D/\Delta f < 0.5\times10^{-6}$ Hz). Thus, based on the Sauerbrey relation NP immobilization on the gold-quartz electrodes resulted in following mass changes: $\Delta m'_{CeO2}$ = (84.6237 ± 0.5664) ng cm^{-2}, $\Delta m'_{Au/CeO2}$ = (46.964 ± 1.062) ng cm^{-2}. Using the mass of one NP and the mass changes per area, the number of NPs per cm^2 is $n_{CeO2}=\Delta m'_{CeO2}/m_{CeO2}$ = $(7.3\pm0.1)\times10^9$ cm^{-2} and $n_{Au/CeO2}$ = $(5.9\pm0.1)\times10^9$ cm^{-2}. This suggests a comparable NP surface loading for both types of NPs. In case of the CeO_2 NPs the percentage of electrode surface coated by NPs can be calculates as the number of NPs per surface area times the cross-section area of one NP (with d_c as derived from Figure 1): $n_{CeO2}\cdot\pi\cdot(d_c(CeO_2)/2)^2 \approx 1.2\%$ (note that here the spherical geometry of the

NPs is neglected and thus a full coverage of 100% would not be possible) For the Au/CeO_2 NPs the surface coverage is $n_{Au/CeO2} \cdot \pi \cdot (d_c(Au/CeO_2)/2)^2 \approx 0.69\%$. This means, that the NP covering density of the Au electrodes is very low. Measurements with the QCM however were recorded under flow conditions within a short time span, in contrast to the electrode preparations for PEC measurements. Furthermore, the Au substrates were not identical for both cases. Thus, for the case of the Au electrodes used for PEC measurements higher coverage with NPs is expected. This was also checked by atomic force microscopy (AFM), in which a significant part of the electrode surface was found to be covered with NPs. A more detailed picture on the NP deposition on the gold electrodes has been obtained by UV/VIS absorption measurements as shown in § IV. All methods however, demonstrate that there is a higher coverage of the electrode with CeO_2 than with Au/ CeO_2 NPs.

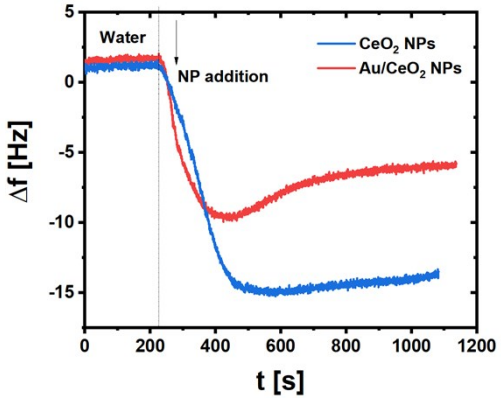

Figure SI-8: *QCM analysis of the adsorption of CeO_2 and Au/CeO_2 NPs on the surface of Au electrodes, forming a single layer structure (Au/cysteamine/NPs). The measurements were carried out at 24 °C using Q-sense to monitor the changes in the resonances frequencies (Δf) and energy dissipation parameters (ΔD), with f = 5 MHz fundamental resonance quartz crystal frequency.*

III) Characterization of nanoparticle deposition in a batch mode with UV/VIS absorption spectroscopy

Adsorption of NPs to the Au electrodes was further characterized by UV/VIS absorption spectroscopy in the air. The absorptions spectrum of Au electrodes modified with cysteamine only were used as reference blank, see Figure SI-9. Changes in absorption after addition of the NPs verified successful deposition of the NPs to the Au electrode. Comparing to the Au electrodes used in the PEC measurements, the Au electrodes used here do not contain a Ti intermediate layer between the glass substrate and the Au film, in order to improve light transmittance. The gold electrodes used here to measure the absorption spectra in air are 500 µm glass/200 nm Au electrodes (Suzhou Research Materials Microtech Co. Ltd, China).

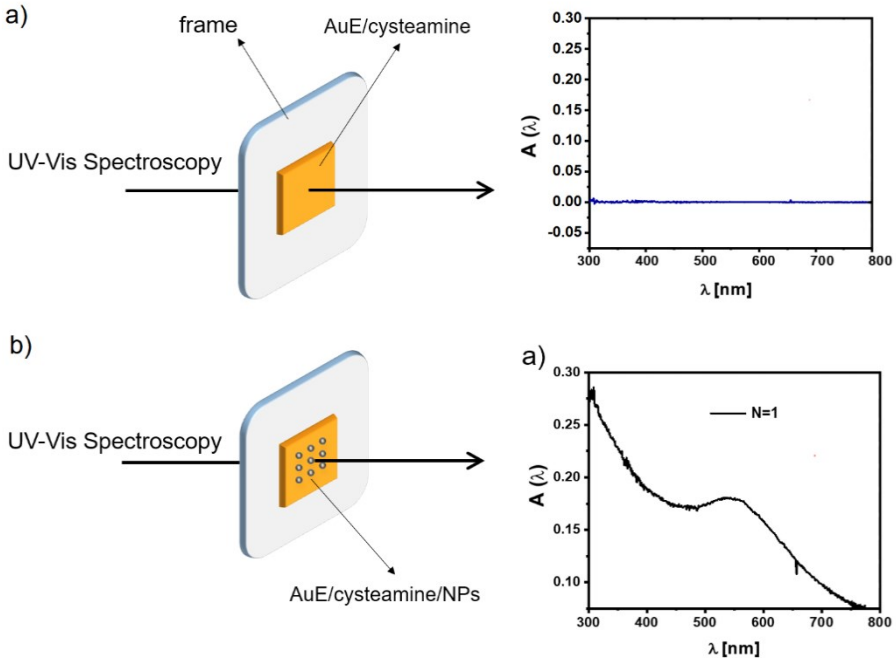

Figure SI-9: *Sketch of the experimental set-up. a) First, a cysteamine modified gold electrode (Au/cysteamine) was fixed on an acrylic frame for obtaining a stable reference spectrum A(λ). b) Afterwards, a single layer of NPs was immobilized on the Au/cysteamine electrode and the absorption spectrum was again recorded, whereby the reference spectrum was used as blank, i.e. was subtracted. The here plotted absorption spectrum A(λ) corresponds to a single layer of Au/CeO_2 NPs.*

IV) Characterization of nanoparticle deposition in multiple layers with UV/VIS absorption spectroscopy

In Figure SI-10 and Figure SI-11 the consecutive absorption spectra as recorded in air upon the subsequent assembly of NP layers are shown. The set-up is the same as shown in Figure SI-9. The absorption at 350 nm *versus* the layer number is shown in Figure 3b of the main manuscript. For the measurements of the absorption spectrum of an electrode with N layers of NPs, the absorption spectrum of the same electrode with N-1 layers of NPs was used as blank. For electrodes with just N = 1 layer of NPs (cf. Figure SI-9), the same electrode without NP layer was used as blank. Due to absorption of the glass substrate of the glass/Au electrode chips, only wavelengths $\lambda > 300$ nm were measured.

Figure SI-10, which has been recorded with CeO_2 NPs, shows no peak in the visible range. Increase of absorption with rising number of layers N demonstrates immobilization of the NPs. In contrast, in Figure SI-11, which has been recorded with Au/CeO_2 NPs, a clear peak can be found around 540 nm, which is due to absorption of the Au cores.

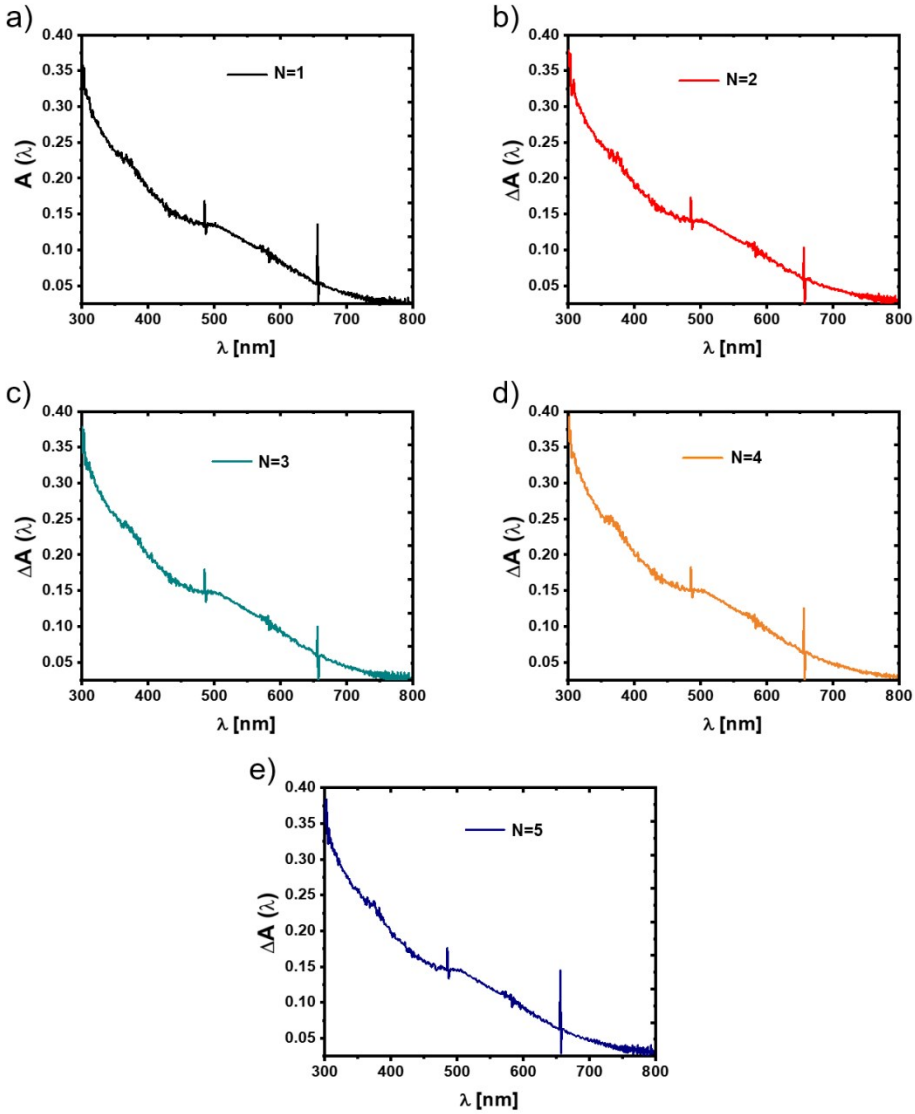

Figure SI-10: *Differential absorption spectrum ΔA(λ) of gold electrodes with N layers of immobilized CeO_2 NPs. The spikes in the spectra are experimental artefacts.*

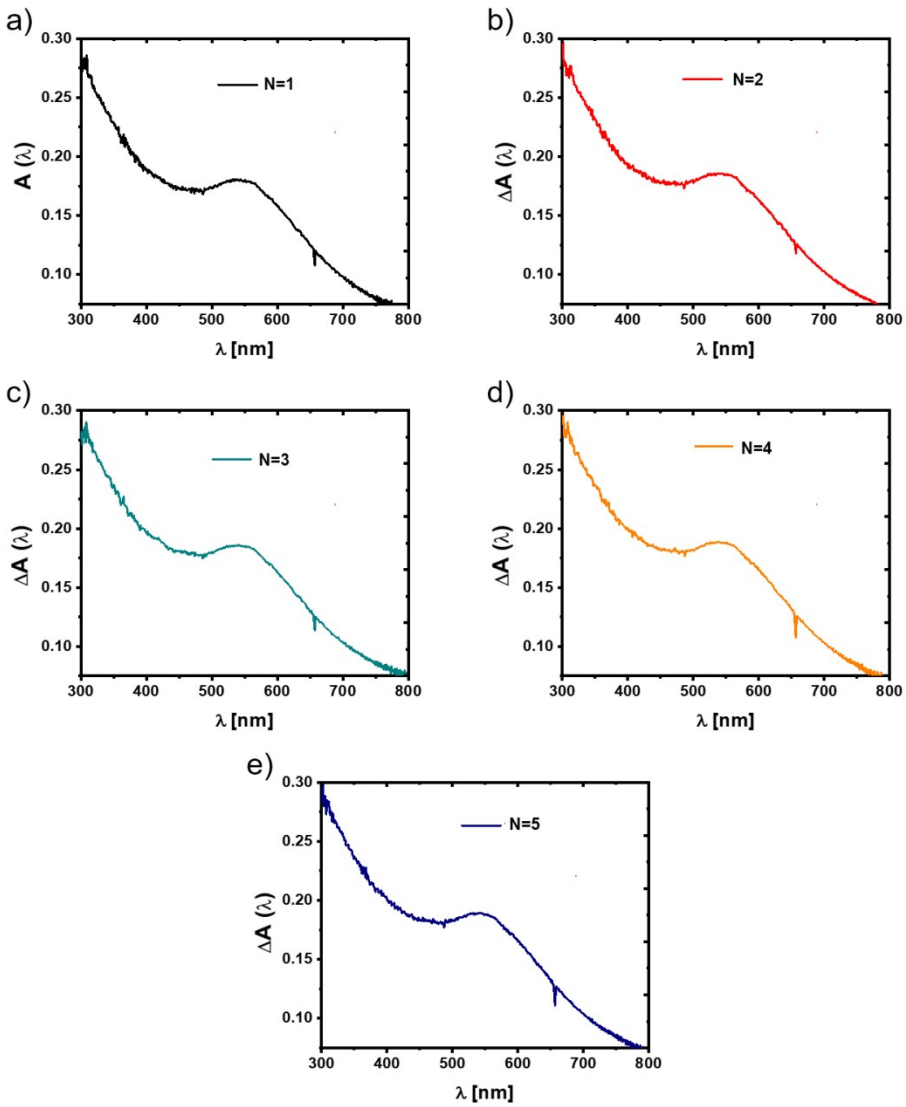

Figure SI-11: *Differential absorption spectrum ΔA(λ) of gold electrodes with N layers of immobilized Au/CeO_2 NPs. The spikes in the spectra are experimental artefacts.*

From the differential absorption spectra of the characterized multilayer structures (Figure 3b, Figure SI-10 and Figure SI-11), the number of NPs of each layer per cm^2 (n) was calculated. The extinction coefficient $\varepsilon(\lambda)$ *[mL·ng^{-1}/cm]* could be calculated from solution spectra $A(\lambda)$, as recorded in a cuvette with pathlength $l_{solution}$ and a volume $V_{solution}$, in which $N_{Au/CeO2}$ Au/CeO_2 NPs are dissolved. Each Au/CeO_2 NP has a mass $m_{Au/CeO2}$ (*cf.* §II), and thus the total mass of NPs in solution is $N_{Au/CeO2} \cdot m_{Au/CeO2}$.

$$A(\lambda) = \varepsilon(\lambda) \cdot c_{Au/CeO2} \cdot l_{solution}$$

$$c_{Au/CeO2} = N_{Au/CeO2} \cdot m_{Au/CeO2} / V_{solution}$$

$$\Rightarrow A(\lambda) = \varepsilon(\lambda) \cdot N_{Au/CeO2} \cdot m_{Au/CeO2} \cdot l_{solution} / V_{solution}$$

$$\Rightarrow \varepsilon(\lambda) = A(\lambda) \cdot V_{solution} / (N_{Au/CeO2} \cdot m_{Au/CeO2} \cdot l_{solution}) = A(\lambda) / (c_{Au/CeO2} \cdot l_{solution})$$

Knowing $\varepsilon(\lambda)$ also allows for determining the number of Au/CeO_2 NPs per area $n_{Au/CeO.}$ For a dried film with thickness l_{film} and volume V_{film}, which comprises $N_{Au/CeO2}$ NPs the absorption is

$$A(\lambda) = \varepsilon(\lambda) \cdot N_{Au/CeO2} \cdot m_{Au/CeO2} \cdot l_{film} / V_{film}$$

V_{film}/l_{film} is the area A_{cross}, on which $N_{Au/CeO2}$ Au/CeO_2 NPs are immobilized, which corresponds to the size of the electrode. The NP density *per* surface area is $n_{Au/CeO2} = N_{Au/CeO2}/A_{cross} = N_{Au/CeO2} \cdot l_{film}/V_{film}$.

$$\Rightarrow A(\lambda) = \varepsilon(\lambda) \cdot m_{Au/CeO2} \cdot n_{Au/CeO2}$$

$$\Rightarrow n_{Au/CeO2} = A(\lambda)/(\varepsilon(\lambda) \cdot m_{Au/CeO2})$$

Instead of deriving $\varepsilon(\lambda)$ from solution spectra it was done here by casting N drops of NP solution (total volume V_{drops}) with concentration $c_{Au/CeO2}$ ($\Rightarrow N_{Au/CeO2} = c_{Au/CeO2} \cdot V_{drops}/m_{Au/CeO2}$) with $N_{Au/CeO2}$ Au/CeO_2 NPs on the electrode and drying them to a film with thickness l_{film} and volume V_{film}. Upon evaporation the number of NPs remains constant, as does the absorption $A(\lambda)$, but the volume is reduced from V_{drop} to V_{film}.

$$A(\lambda) = \varepsilon(\lambda) \cdot N_{Au/CeO2} \cdot m_{Au/CeO2} \cdot l_{film} / V_{film} = \varepsilon(\lambda) \cdot (c_{Au/CeO2} \cdot V_{drops}/m_{Au/CeO2}) \cdot m_{Au/CeO2} \cdot l_{film} / V_{film}$$
$$= \varepsilon(\lambda) \cdot c_{Au/CeO2} \cdot V_{drops} \cdot l_{film} / V_{film} = \varepsilon(\lambda) \cdot c_{Au/CeO2} \cdot V_{drops}/A_{chip}$$

$V_{film}/l_{film} = A_{chip}$ is the area of the electrode covered with the NP film, which is constant for all measurements. The active area of the electrode is a circle with diameter 0.6 cm, *i.e.* $A_{chip} = 0.28\ cm^2$.

$$\Rightarrow \varepsilon(\lambda) = A(\lambda) \cdot A_{chip}/(c_{Au/CeO2} \cdot V_{drops})$$

Again, the surface coverage of such a film is

$$n_{Au/CeO2} = A(\lambda)/(\varepsilon(\lambda) \cdot m_{Au/CeO2})$$

Thus, by measuring the absorption spectrum the surface coverage $n_{Au/CeO2}$ of the NPs can be calculated. This is shown for the Au/CeO_2 NP and the CeO_2 NP films in Table SI-2 and Table SI-3.

Hybrid Au/CeO_2 NPs on the Au electrode ($m_{Au/CeO2} = 8.034\times10^{-18}$ g, $A_{chip} = 0.28$ cm^2)

Method	N	V_{drops} [uL]	$c_{Au/CeO2}$ [ng·mL^{-1}]	$A(\lambda)$ (λ = 300 nm)	$\varepsilon(\lambda)$ [cm^2·ng^{-1}]	$n_{Au/CeO2}$ [cm^{-2}]
casting N drops of NP solution followed by drying	1	30	10740	0.36	3.13×10^{-4}	1.43×10^{11}
	2	60	10740	0.54	2.34×10^{-4}	2.88×10^{11}
	3	90	10740	0.77	2.23×10^{-4}	4.32×10^{11}
					2.57×10^{-4} (mean)	
Method	N	-	-	$A(\lambda)$ (λ = 300 nm)	$\varepsilon(\lambda)$ [cm^2·ng^{-1}]	$n_{Au/CeO2}$ [cm^{-2}]
Differential absorption from multilayer structure with N layers as used in Figure SI-11	1	-	-	0.28	2.57×10^{-4}	1.36×10^{11}
	2	-	-	0.3		1.46×10^{11}
	3	-	-	0.28		1.36×10^{11}
	4	-	-	0.3		1.46×10^{11}
	5	-	-	0.29		1.41×10^{11}
						1.41×10^{11} (mean)

Table SI-2: The calculations of the extinction coefficient $\varepsilon(\lambda=300\ nm)$ and the number of Au/CeO_2 NPs per cm^2 ($n_{Au/CeO2}$) on the Au electrode.

CeO_2 NPs on the Au electrode ($m_{CeO2} = 11.5\times10^{-18}$ g, $A_{chip} = 0.28$ cm²)

Method	N	V_{drops} [uL]	c_{CeO2} [ng·mL^{-1}]	$A(\lambda)$ (λ = 300 nm)	$\varepsilon(\lambda)$ [cm^2·ng^{-1}]	n_{CeO2} [cm^{-2}]
casting N drops of NP solution followed by drying	1	30	18627	0.18	0.902×10^{-4}	1.74×10^{11}
	2	60	18627	0.31	0.777×10^{-4}	3.47×10^{11}
	3	90	18627	0.47	0.785×10^{-4}	5.21×10^{11}
					0.821×10^{-4} (mean)	
Method	N	-	-	$A(\lambda)$ (λ = 300 nm)	$\varepsilon(\lambda)$ [cm^2·ng^{-1}]	n_{CeO2} [cm^{-2}]
Differential absorption from multilayer structure with N layers as used in Figure SI-10	1	-	-	0.36	0.821×10^{-4}	3.81×10^{11}
	2	-	-	0.38		4.02×10^{11}
	3	-	-	0.38		4.02×10^{11}
	4	-	-	0.4		4.24×10^{11}
	5	-	-	0.38		4.02×10^{11}
						4.02×10^{11} (mean)

Table SI-3: The calculations of the extinction coefficient $\varepsilon(\lambda=300\ nm)$ and the number of CeO_2 NPs per cm² ($n_{Au/CeO2}$) on the Au electrode.

From the NP surface densities $n_{CeO2} = 4.02\times10^{11}\ cm^{-2}$ and $n_{Au/CeO2} = 1.41\times10^{11}\ cm^{-2}$ the surface coverages $n_{CeO2}\cdot\pi\cdot(d_c(CeO_2)/2)^2 \approx 66\%$ and $n_{Au/CeO2}\cdot\pi\cdot(d_c(Au/CeO_2)/2)^2 \approx 16\%$ could be calculated analogous to §II. In agreement with the QCM measurements from §II these data show higher coverage of the electrode with CeO_2 than with Au/CeO_2 NPs. However, the absorption spectrum data (which were recorded without flow) show much higher surface coverage than the QCM data (which were recorded with flow), and these numbers correspond better to the qualitative AFM data.

V) Description of the used experimental set-up for measuring photocurrents

Photocurrents were measured by a homebuilt photoelectrochemical system, whose photograph is shown in Figure SI-12. A detailed scheme of the set-up is shown in Figure SI-13. This system is based on previous set-ups[4-7]. A Faraday cage was used for eliminating electromagnetic interference.

A potentiostat from CH Instruments was used to apply a constant bias voltage U with a three-electrode system, including the working electrode (WE) of gold covered with the NPs, a counter electrode (CE) of Pt, and a reference electrode (RE) of Ag/AgCl 3 M NaCl. Photocurrents were amplified and rectified with a lock-in amplifier (EG&G Model # 5210). After that, the photocurrent was read in by a computer using LabVIEW software.

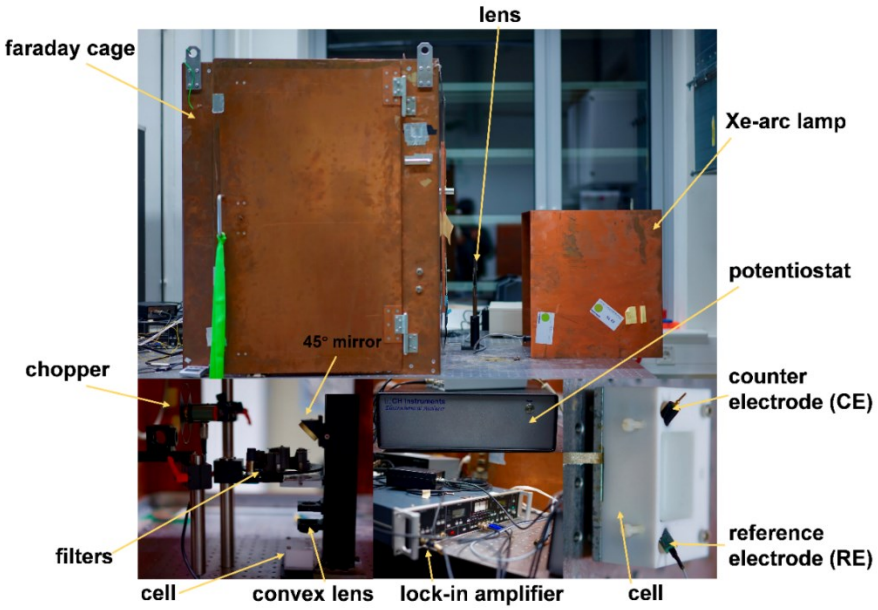

Figure SI-12: *Photograph of the homebuilt PEC system.*

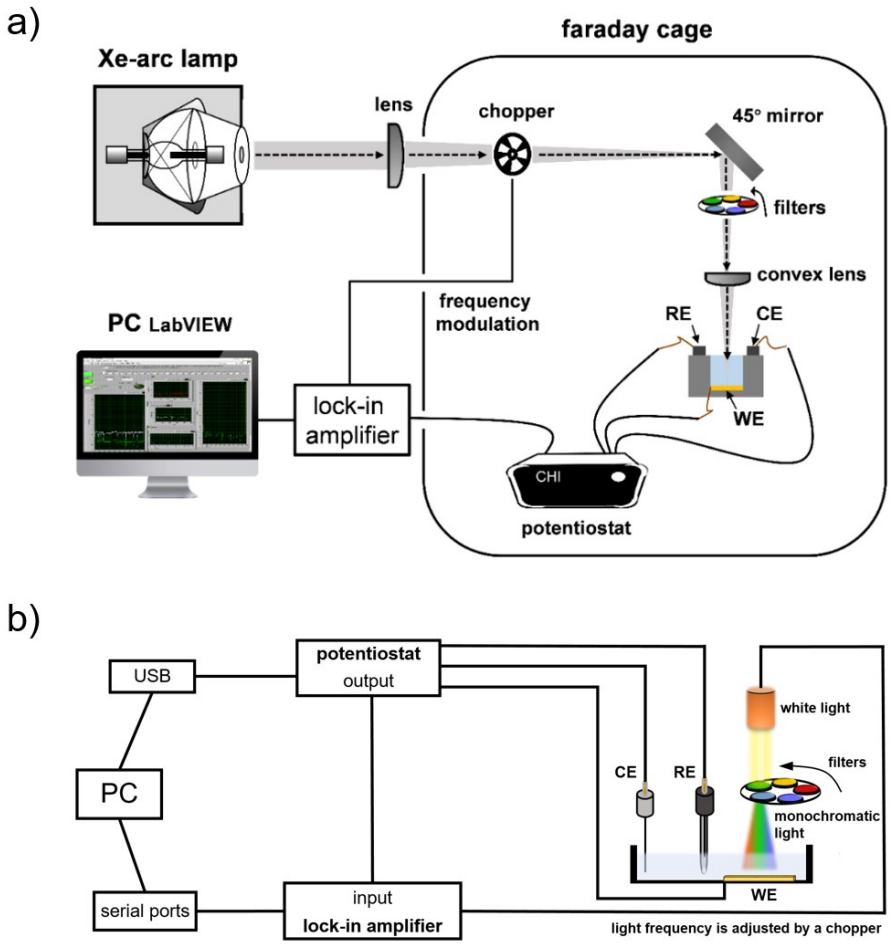

Figure SI-13: *a) Scheme of the photoelectrochemical system. b) The diagram of the photoelectrochemical measurement system. The working electrode (WE) was a gold electrode modified with CeO_2 or Au/CeO_2 core/shell hybrid NPs. A Pt wire and an Ag/AgCl (3 M NaCl) electrode were used as counter electrode (CE) and reference electrode (RE), respectively.*

A detailed description of the teflon cell is shown in Figure SI-14a. The WE was fixed and well-sealed by an o ring between a teflon and aluminum sheet with the help of four screws. Conductive tapes were used electrically connect the WE for recording of the generated photocurrents. The hole size of the teflon cell was 6 mm, which determined the size of the illuminated spot of the WE ($A_{chip} \approx 0.28$ cm^2).

A Xe-arc lamp (Ushio, Inc., Japan) was applied as white light source from 250 nm to 1100 nm. Focused by several lenses and modulated by a chopper, the light beam with 6 mm diameter spot size was finally illuminating the working electrode surface in a teflon cell. The modulation frequency was chosen as 71 Hz, which also was used as reference frequency of the lock-in amplifier. Different optical filters were used to obtain different colors from the white light. The filters were 340 ± 26 nm (BrightLine), 405 ± 10 nm (BrightLine), 470 ± 40 nm (CHROMA), 540 ± 25 nm (CHROMA), 620 ± 20

nm (CHROMA), 725 ± 50 nm (CarlZeiss), and 870 ± 50 nm (CHROMA). These band-pass filters allowed for transmission of ca. 80%-90% of the light intensity at the respective wavelengths. We did not measure the specific power hitting the electrode surface. The white light spectral distribution of the Xe-arc lamp is shown in Figure SI-14b.

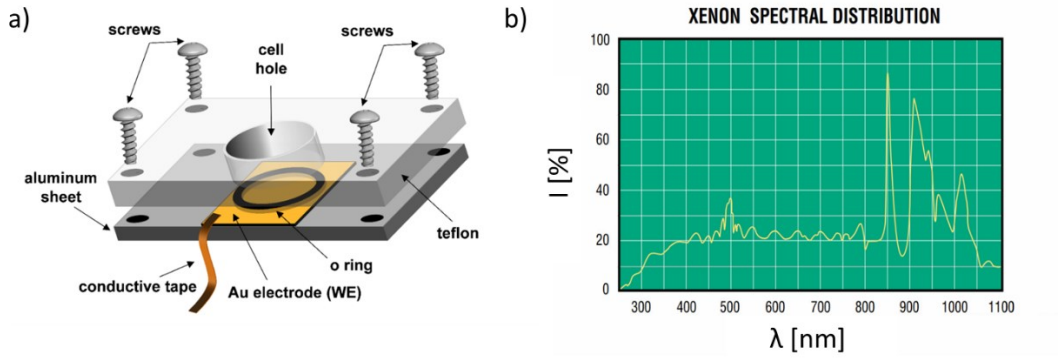

Figure SI-14: a) *Sketch of the electrochemical cell used in this work. b) Spectral distribution of the used Xe-arc lamp given as wavelength-dependent relative intensity I(λ). This image has been taken from the webpage of the manufacturer (https://www.ushio.com/product/uxl-xenon-short-arc/).*

VI) Photocurrent measurements

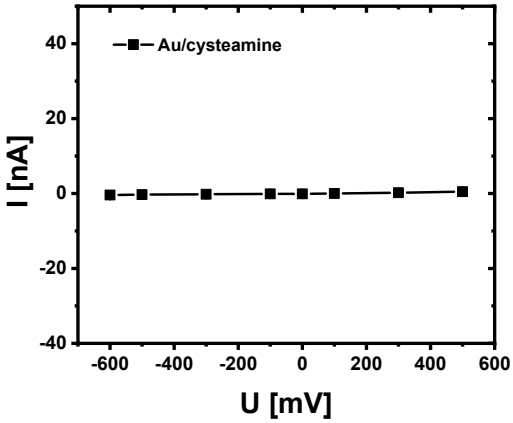

Figure SI-15: *Photocurrent at different bias potentials U recorded in 0.01 M PBS under white light illumination with Au/cysteamine electrodes without immobilized NPs.*

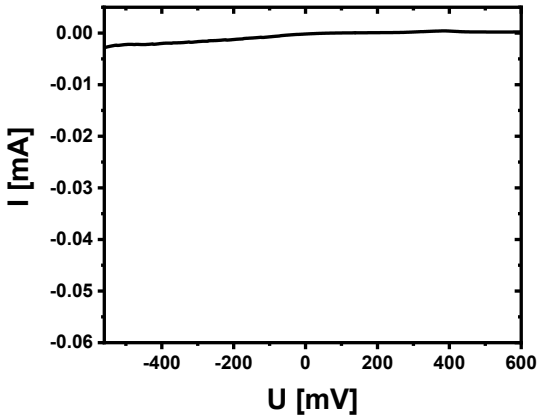

Figure SI-16: *Chopped light voltammetry of gold electrodes modified with 5 layers of Au NPs in PBS with 5 mM H_2O_2.*

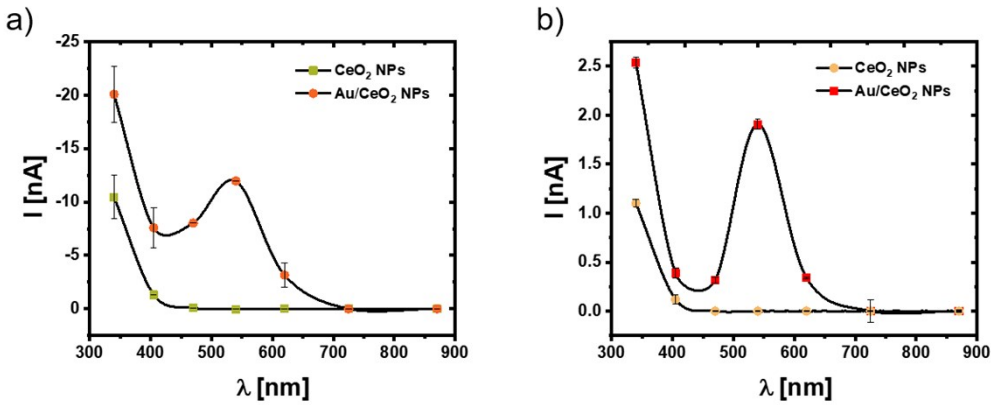

Figure SI-17: *Wavelength dependence of the photocurrent I(λ) recorded on Au electrodes modified with N = 5 layers CeO_2 NPs or 5 layers Au/CeO_2 NPs at a) U = -*

300 and b) U = 300 mV vs. Ag/AgCl in 0.01 M PBS under illumination with light of different wavelengths λ.

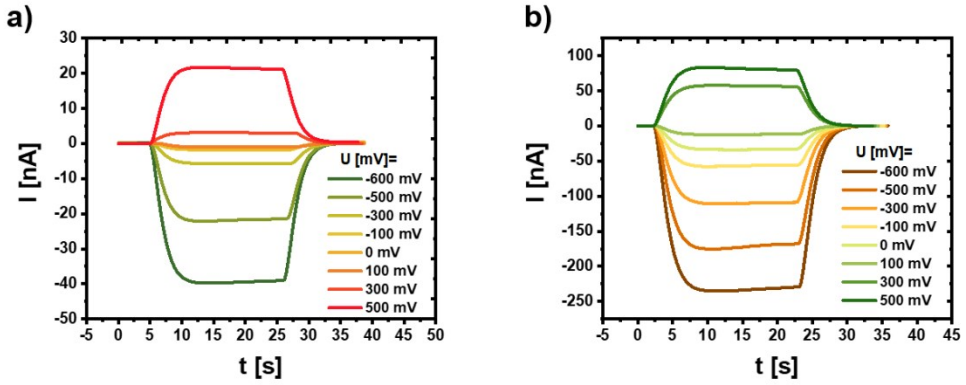

Figure SI-18: *Transient photocurrents I(t) at different bias potential U vs. Ag/AgCl from a) N = 5 layers CeO_2 NPs and b) N = 5 layers Au/CeO_2 NPs in 0.01 M PBS under illumination of white light.*

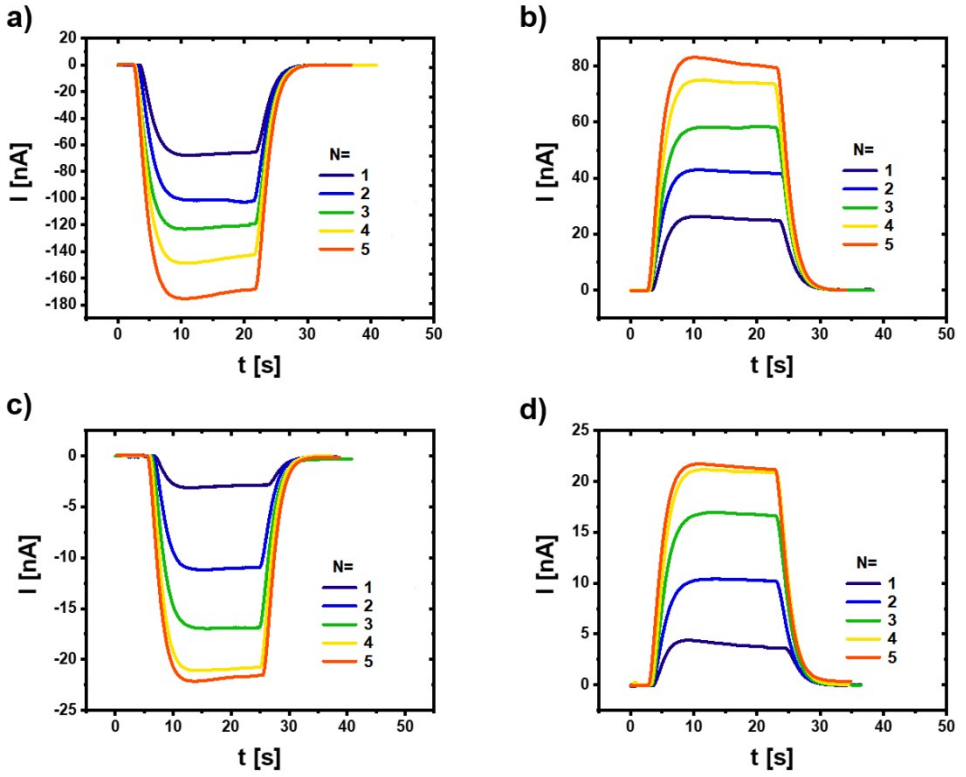

Figure SI-19: *Transient photocurrents I(t) as recorded on Au electrodes with different numbers N of NP layers and different bias potential U under white light illumination in 0.01 PBS. a) Au/CeO_2 NPs at U -500 mV. b) Au/CeO_2 NPs at U = 500 mV, c) CeO_2 NPs at U = -500 mV. d) CeO_2 NPs at U = 500 mV vs. Ag/AgCl.*

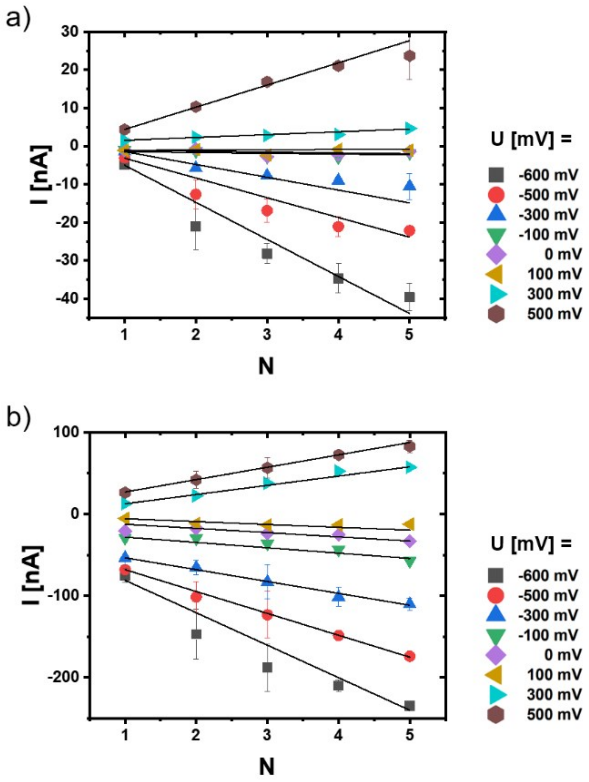

Figure SI-20: *Photocurrents I as recorded under white light in 0.01 M PBS pH=7.4 of Au electrodes modified with N layers of a) CeO_2 NPs and b) Au/CeO_2 NPs at different potentials U.*

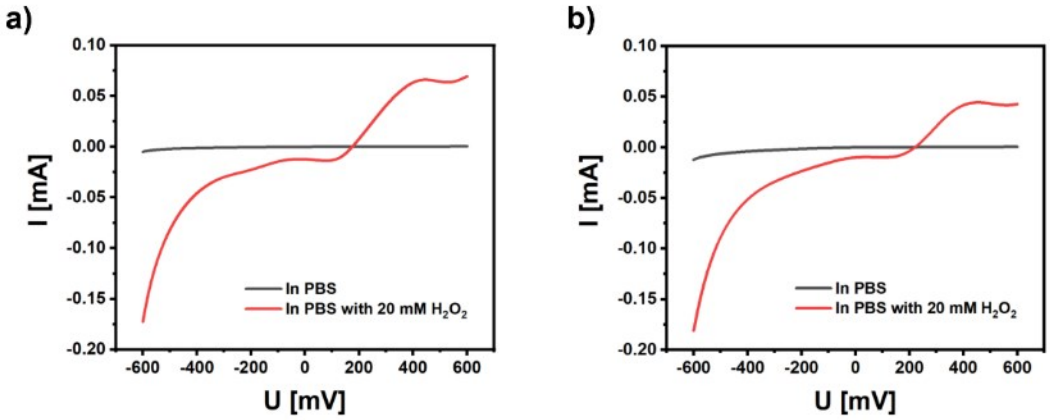

Figure SI-21: Cyclic voltammetric measurements without light of (a) 5 layers CeO_2 NPs and (b) 5 layers Au/CeO_2 NPs immobilised on gold electrodes in 100 mM PBS buffer pH = 7.4 and in buffer with 20 mM H_2O_2 using potential scanning from -600 mV to 600 mV vs Ag/AgCl. The scan rate was 5 mV/s.

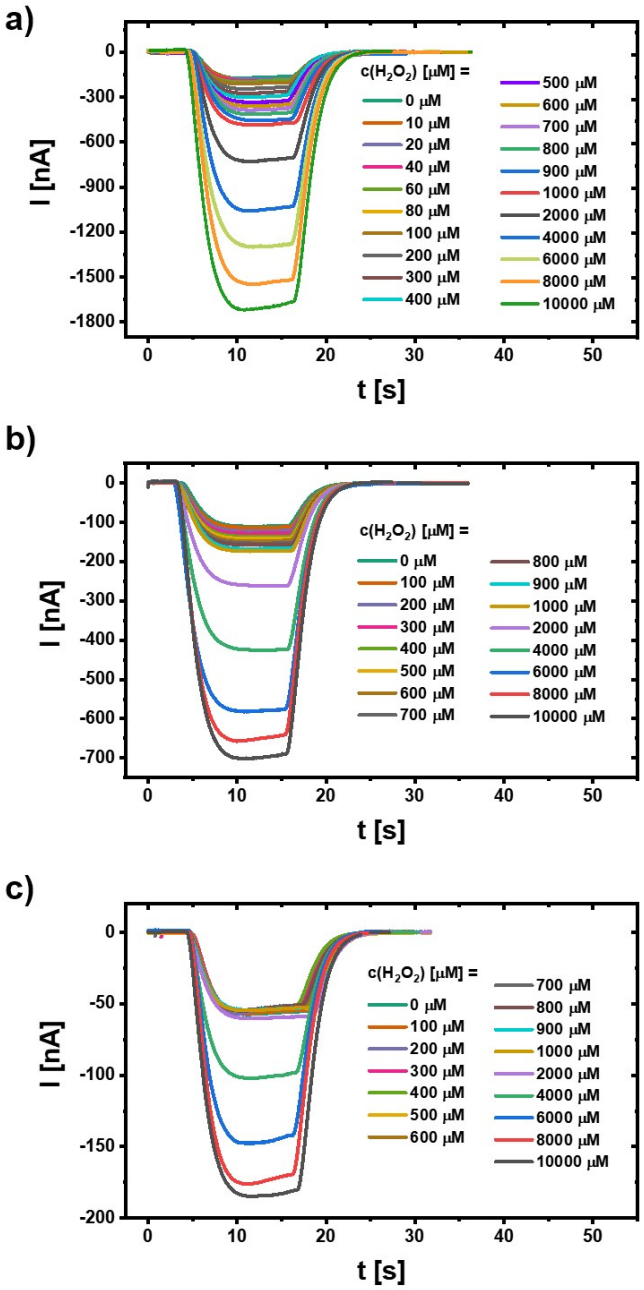

Figure SI-22: *Transient photocurrents I(t) recorded under while light illumination at different H_2O_2 concentrations c(H_2O_2) recorded on Au electrodes with N = 5 layers of Au/CeO_2 NPs. The bias potentials U vs. Ag/AgCl with 3 M NaCl were a) -500 mV, b) -300 mV, and c) -100 mV.*

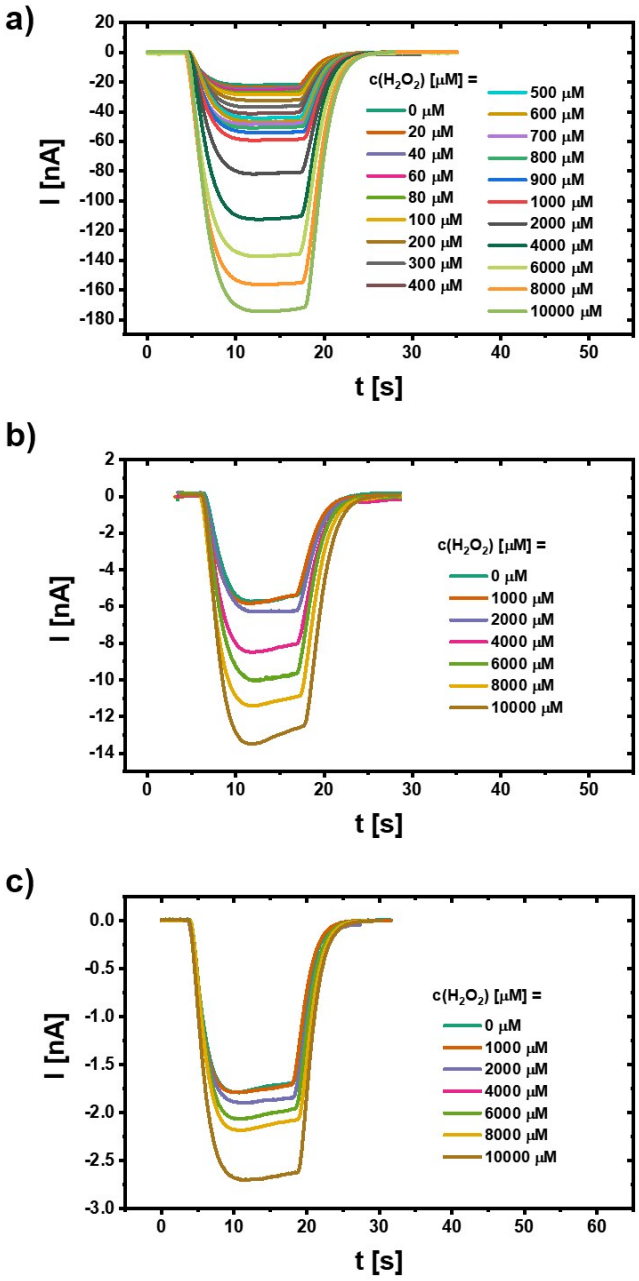

Figure SI-23: *Transient photocurrents I(t) recorded under while light illumination at different H_2O_2 concentrations c(H_2O_2) recorded on Au electrodes with N = 5 layers of CeO_2 NPs. The bias potentials U vs. Ag/AgCl with 3 M NaCl were a) -500 mV, b) -300 mV, and c) -100 mV.*

Method	Material	LOD	Linear range	Sensitivity	Reference
PEC	Cu_2O/CoP nanostructures	100 nM	20-220 µM	16 mA cm^{-2} mM^{-1}	[8]
PEC	Au NCs	2000 nM	30-5000 µM	131 nA cm^{-2} mM^{-1}	[9]
PEC	PbS/C_3N_4 NPs	1050 nM	10-7000 µM	-	[10]
PEC	NiOOH/Pt/Si nanostructures	2200 nM	10-60 mM	-	[11]
PEC	CeO_2 NPs	27 µM	50-1000 µM	126 nA cm^{-2} mM^{-1}	This work
PEC	Au/CeO_2 NPs	3 µM	4-2000 µM	1150 nA cm^{-2} mM^{-1}	This work

Table SI-4: *Comparison of the H_2O_2 sensing performance of different methods. CNTs = carbon nanotubes. NCs = nano clusters.*

VII) Stability and interference measurements

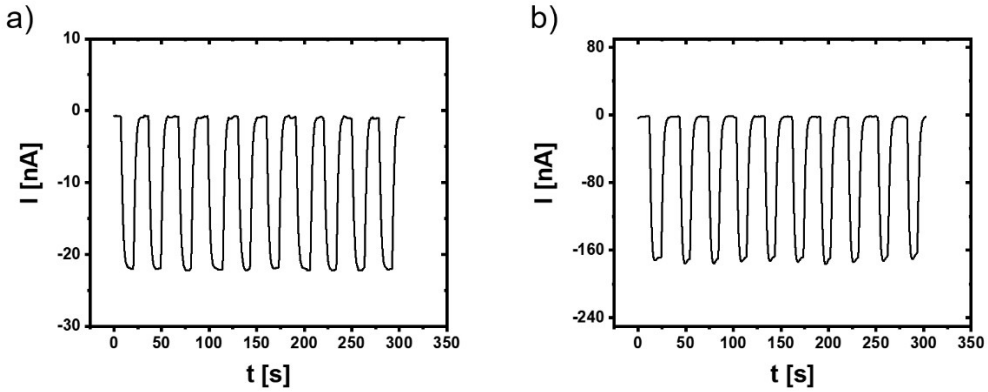

Figure SI-24: *Measurements of the photocurrent stability I(t) within 300 s with Au electrodes with a) N = 5 layers CeO_2 NPs and b) 5 layers Au/CeO_2 NPs, carried out in 0.01 M PBS pH 7.4 under white light illumination, with a bias U = -500 mV.*

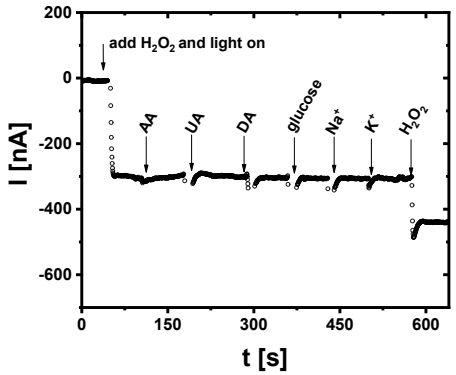

Figure SI-25: *Photocurrent response of an Au electrode with N = 5 layers Au/CeO_2 NPs immersed in 0.01 M PBS (pH=7.4) upon successively adding H_2O_2 (final concentration c(H_2O_2) = 1 mM after addition), dopamine (DA) (final concentration 1 mM after addition), ascorbic acid (AA), uric acid (UA), glucose, NaCl and KCl (final concentratin 10 mM after each addition) at U = -500 mV vs. Ag/AgCl under white light illumination.*

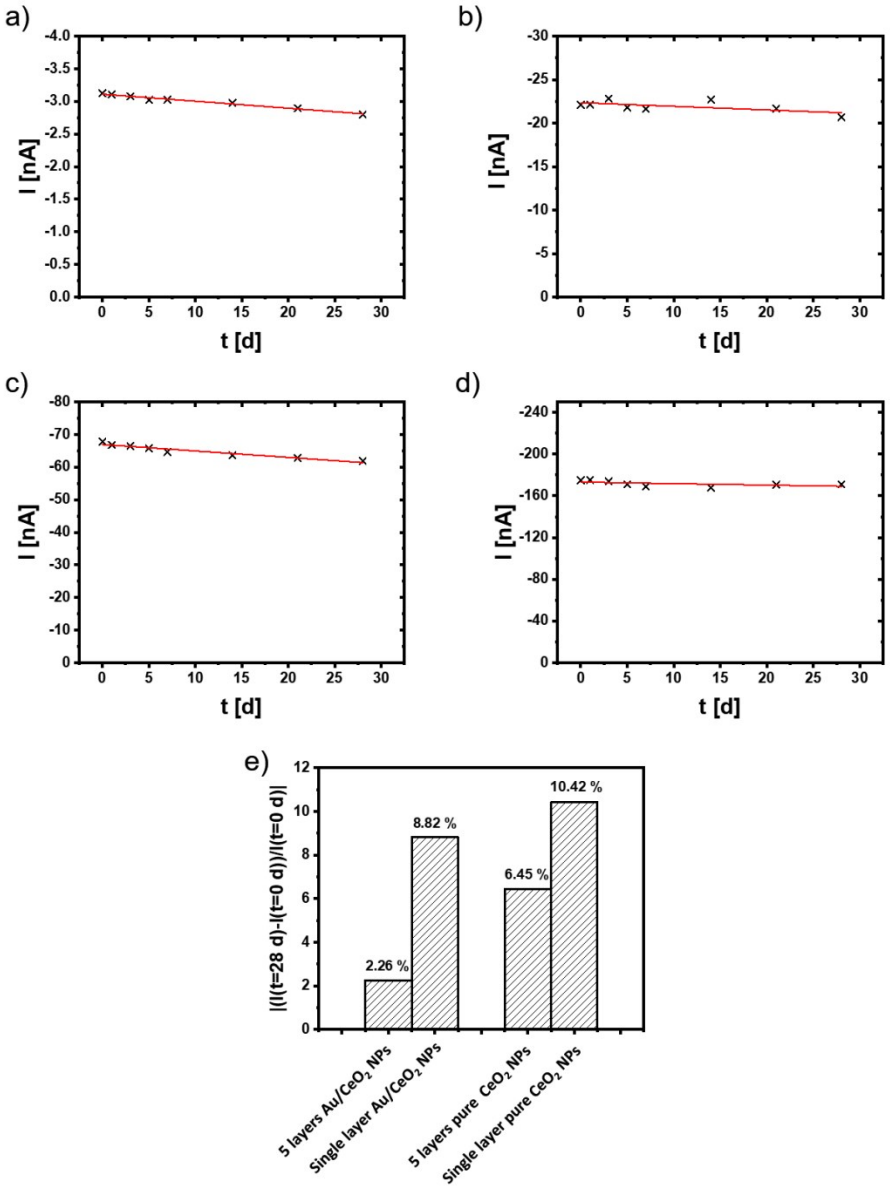

Figure SI-26: *Verification of the storage stability of NP coated Au electrodes. The photocurrent response from Au electrodes immobilized with a) N = 1 single layer CeO_2 NPs, b) N = 5 multilayers CeO_2 NPs, c) N = 1 single layer Au/CeO_2 NPs, and d) N = 5 multilayers Au/CeO_2 NPs in 0.01 M PBS (pH=7.4) after having stored the electrodes for the time t at 4 °C. Photocurrents were recorded at U = -500 mV vs. Ag/AgCl under white light illumination. e) Percentual loss of photocurrent after t = 28 days storage.*

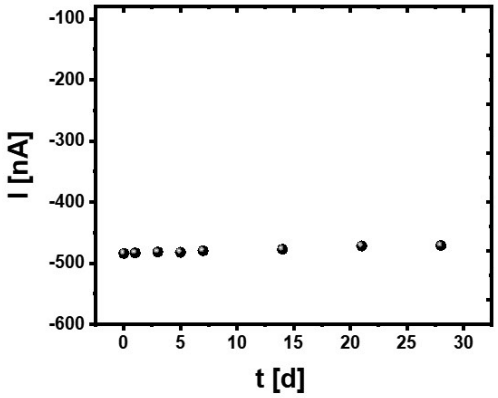

Figure SI-27: *Stability of photocurrent response after different storage times t (in PBS at 4 °C) of Au electrodes with N = 5 layers Au/CeO_2 hybrid NPs in 1 mM H_2O_2, recorded at U = -500 mV vs. Ag/AgCl under white light illumination. The 5 layers Au/CeO_2 electrode is storage for different time.*

VII) References

1. N. G. Bastús, J. Piella, S. Perez, J. Patarroyo, A. Genc, J. Arbiol and V. Puntes, *Applied Materials Today*, 2019, **15**, 445-452.
2. J. Hühn, C. Carrillo-Carrion, M. G. Soliman, C. Pfeiffer, D. Valdeperez, A. Masood, I. Chakraborty, L. Zhu, M. Gallego, Y. Zhao, M. Carril, N. Feliu, A. Escudero, A. M. Alkilany, B. Pelaz, P. d. Pino and W. J. Parak, *Chem. Mater.*, 2017, **29**, 399−461.
3. M. M. O. Thotiyl, H. Basit, J. A. Sánchez, C. Goyer, L. Coche-Guerente, P. Dumy, S. Sampath, P. Labbé and J.-C. Moutet, *J. Colloid Interface Sci.*, 2012, **383**, 130-139.
4. S. Zhao, J. Völkner, M. Riedel, G. Witte, Z. Yue, F. Lisdat and W. J. Parak, *Applied Materials and Interfaces*, 2019, **11**, 21830−21839.
5. N. Sabir, N. Khan, J. Völkner, F. Widdascheck, P. d. Pino, G. Witte, M. Riedel, F. Lisdat, M. Konrad and W. J. Parak, *SMALL*, 2015, **43**, 5844–5850.
6. W. Khalid, M. E. Helou, T. Murböck, Z. Yue, J.-M. Montenegro, K. Schubert, G. Göbel, F. Lisdat, G. Witte and W. J. Parak, *ACS Nano*, 2011, **5**, 9870-9876.
7. Z. Yue, W. Khalid, M. Zanella, A. Z. Abbasi, A. Pfreundt, P. Rivera_Gil, K. Schubert, F. Lisdat and W. J. Parak, *Anal. Bioanal. Chem.*, 2010, **396**, 1095-1103.
8. J. Tian, H. Zhu, J. Chen, X. Zheng, H. Duan, K. Pu and P. Chen, *Small*, 2017, **12**, 1700798.
9. Z. Shuang, Z. Jun, L. Zhengping, Z. Peixin and L. Yunxiao, *Microchimica Acta*, 2017, **184**, 1-10.
10. R. Li, Y. Zhang, W. Tu and Z. Dai, *ACS Appl. Mater. Interfaces*, 2017, **9**, 22289-22297.
11. H. Li, W. Hao, J. Hu and H. Wu, *Biosens. Bioelectron.*, 2013, **47**, 225-230.